Front. Mater. Sci. 2023, 17(2): 230647
https://doi.org/10.1007/s11706-023-0647-7

RESEARCH ARTICLE

Fabrication of glycidyl methacrylate-modified silk fibroin/poly(L-lactic acid-co-ε-caprolactone)–polyethylene glycol diacrylate hybrid 3D nanofibrous scaffolds for tissue engineering

Yongyong Fan[1,2], Anlin Yin[2], Yunhuan Li[1,2], Qi Gu[2], Yan Zhou[2], Junlong Zhou[2], Ruibo Zhao (✉)[1], and Kuihua Zhang (✉)[2]

1 Institute of Smart Biomaterials, School of Materials Science and Engineering and Zhejiang-Mauritius Joint Research Center for Biomaterials and Tissue Engineering, Zhejiang Sci-Tech University, Hangzhou 310018, China
2 College of Materials and Textile Engineering, Nanotechnology Research Institute, Jiaxing University, Jiaxing 314001, China

ABSTRACT: In order to provide a biomimetic natural extracellular matrix microenvironment with excellent mechanical capacity for tissue regeneration, a novel porous hybrid glycidyl methacrylate-modified silk fibroin/poly(L-lactic acid-co-ε-caprolactone)–polyethylene glycol diacrylate (SFMA/P(LLA-CL)–PEGDA) hybrid three-dimensional (3D) nanofibrous scaffolds was successfully fabricated through the combination of 3D nanofibrous platforms and divinyl PEGDA based photocrosslinking, and then further improved water resistance by ethanol vapor post-treatment. Scanning electron microscopy and micro-computed tomography results demonstrated significant PEGDA hydrogel-like matrices bonded nanofibers, which formed a 3D structure similar to that of "steel bar (nanofibers)–cement (PEGDA)", with proper pore size, high porosity, and high pore connectivity density. Meanwhile, the hybrid 3D nanofibrous scaffolds showed outstanding swelling properties as well as improved compressive and tensile properties. Furthermore, these hybrid 3D nanofibrous scaffolds could provide a biocompatible microenvironment, capable of inducing the material–cell hybrid and regulating human umbilical vein endothelial cells proliferation. They thus present significant potential in tissue regeneration.

KEYWORDS: hybrid 3D nanofibrous scaffold; silk fibroin; tissue engineering; human umbilical vein endothelial cell

Contents

1 Introduction
2 Experimental
  2.1 Materials
  2.2 Fabrication of SFMA
  2.3 Preparation of hybrid 3D nanofibrous scaffolds
  2.4 Characterization
  2.5 Property determination of hybrid 3D nanofibrous scaffolds
  2.6 Statistical analysis
3 Results and discussion
  3.1 Characterization of SFMA

Received February 8, 2023; accepted April 2, 2023

E-mails: zhangkuihua@126.com (K.Z.), rzhao@zstu.edu.cn (R.Z.)

3.2 Effect of different crosslinking methods on hybrid 3D nanofibrous scaffolds
3.3 Thermal analyses of hybrid 3D nanofibrous scaffolds
3.4 Morphologies and microstructures of hybrid 3D nanofibrous scaffolds
3.5 Swelling properties of hybrid 3D nanofibrous scaffolds
3.6 Mechanical properties of hybrid 3D nanofibrous scaffolds
3.7 *In vitro* biocompatibility of hybrid 3D nanofibrous scaffolds
4 Conclusions
Disclosure of potential conflicts of interests
Acknowledgements
Electronic supplementary information
References

1 Introduction

Tissue engineering scaffolds with the mimetic function of extracellular matrix (ECM) have demonstrated great potential in tissue regeneration [1]. The ideal tissue engineering scaffolds should imitate natural ECM, in terms of components and structures, to facilitate cell adhesion, proliferation, migration, and differentiation to the maximum extent [2–3]. Moreover, biomimetic ECM has the potential to regulate the biological behavior of related growth cells, angiogenesis, and tissue regeneration [4]. Various studies have shown that materials with chemical composition similar to that of natural ECM, such as collagen, chitosan, laminin, and silk fibroin (SF), significantly improved the biocompatibility of scaffolds [5–6]. SF, as a natural protein extracted from silkworm cocoons, has been widely applied in tissue engineering owing to its numerous virtues such as excellent biocompatibility, good air and moisture permeability, non-immunogenicity, and cost-efficiency, and can be fabricated into films, hydrogels, electrospun membranes, and porous sponges for regenerative medicine [7–11]. In our previous study, electrospun nanofibrous scaffolds of SF and its blends achieved good biocompatibility and biodegradability for wound dressing and peripheral nerve regeneration. Furthermore, the nanofibrous scaffolds with SF greatly enhanced the adhesion and proliferation of endothelial cells and significantly improved the number and quality of new blood vessels in the scaffolds [12–13]. However, the conventional electrospun two dimensional (2D) structural scaffolds with small pore size and poor normalized pore connectivity restricted the transport of nutrients and metabolites and cellular infiltration, further influencing cell ingrowth [14–15].

Currently, three-dimensional (3D) structural electrospun nanofibrous scaffolds with proper pore size, high porosity, and pore connectivity have attracted increasing attention in tissue engineering fields [16–17]. They promote cell infiltration and transport of nutrients and metabolites. Moreover, they can increase the effective contact area of scaffolds' inner surface to induce cellar stretching and migration as well as the growth of peripheral blood vessels [18–21]. The fabrication method of 3D electrospun nanofibrous scaffolds mainly involves multilayering, sacrificial agent, dynamic liquid, and ultrasound-enhanced electrospinning, as well as post-processing [14,22]. In comparison with other methods, the post-processing of nanofibers is more conducive to adjusting shape and physicochemical properties, as is desirable for repairing different tissues [23–24]. Xu et al. [25] fabricated porous polycaprolactone (PCL) 3D nanofibrous scaffolds via thermal-induced self-agglomeration of fragmented electrospun nanofibers followed by freeze-drying, promoting bone morphogenetic protein 2 (BMP-2)-induced chondrogenic nanofibrous scaffolds for bone generation. Sun et al. [26] reported that the SF/poly (L-lactic acid-co-ε-caprolactone) (P(LLA-CL)) porous nanofibrous sponges (NSs) were fabricated through fragmented electrospun nanofiber homogenization, freeze-drying, crosslinked by glutaraldehyde vapor, and then filled into nerve guidance conduits (NGCs). This kind of NSs-containing NGCs was more beneficial to cell growth, blood vessel formation, and nerve regeneration compared with 2D nanofibrous scaffolds. In our previous study, a double-layer neural scaffold consisted of porous 3D nanofibrous scaffold via fragmented electrospun nanofiber homogenization, mold forming, freeze-drying, and then crosslinked by glutaraldehyde vapor as the primary layer (inner layer), with electrospun P(LLA-CL)/polyoxyethylene (PEO) micronanofiber film as the outer layer to improve mechanical support. The biological evaluation *in vitro* and *in vivo* showed that these porous 3D neural scaffolds' ability to promote vascularization and nerve regeneration was significantly better than that of electrospun 2D nanofibrous scaffolds [27]. However, the mechanical properties of the internal porous 3D nanofibrous scaffold made of fragmented nanofibers

crosslinked by glutaraldehyde vapor could not fulfill the requirements of most tissue repair, and the glutaraldehyde presented a certain cytotoxicity [28]. Recently, polyethylene glycol diacrylate (PEGDA) has been utilized as 3D printing hydrogel ink to manufacture scaffolds suitable for application relating to cells and biomolecules, this method offers good biocompatibility, biodegradability, good crosslinking and bonding effect [29]. Zhu et al. reported that the mechanical properties of the 3D printing gelatin methacrylate (GelMA)–PEGDA composite hydrogel could be regulated by the molecular weight, concentration, exposure intensity, and exposure duration of PEGDA [30–31].

In the present study, firstly, glycidyl methacrylate-modified silk fibroin (SFMA) was prepared by graft modification of SF with glycidyl methacrylate (GMA) to introduce methacrylate, and then SFMA and P(LLA-CL) blends were electrospun to obtain SFMA/P(LLA-CL) nanofibrous membranes. Secondly, a novel porous SFMA/P(LLA-CL)–PEGDA 3D hybrid nanofibrous scaffold similar to "steel bar (nanofiber)–cement (PEGDA)" structure, namely fiber-reinforced polymer matrix composite structure, was constructed through the combination of the preparation technology of 3D nanofibrous scaffolds and the use of divinyl PEGDA as photocrosslinking agent and binder. Finally, human umbilical vein endothelial cells (HUVECs) were cultured on SFMA/P(LLA-CL)–PEGDA hybrid 3D nanofibrous scaffolds to estimate the cytocompatibility. These hybrid 3D nanofibrous scaffolds were expected to improve mechanical properties and closely mimic the structure of ECM to promote tissue regeneration.

2 Experimental

2.1 Materials

Cocoons of silkworms (*Bombyx mori*) were kindly donated by Jiaxing Silk Co., Ltd. (Zhejiang, China). A copolymer of P(LLA-CL) (50:50) containing 50 mol.% L-lactide was purchased from Jinan Daigang Co., Ltd. (Shandong, China). PEGDA (Mn = 1000), GMA, photoinitiator lithium phenyl-2,4,6-trimethylbenzoylphosphinate (LAP), 1,1,1,3,3,3-hexafluoro-2-propanol (HFIP), lithium bromide (LiBr), and tert-butyl alcohol (t-BuOH) were bought from Shanghai Aladdin Technology Co., Ltd. (Shanghai, China). The cells were supplied by Shanghai Cell Bank (China). Cell culture reagents were acquired from Gibco (UK).

2.2 Fabrication of SFMA

Raw silk was degummed three times, each for 30 min, with 0.5% (w/w) Na_2CO_3 solution at 100 °C and then washed with distilled water and dried to obtain degummed SF. Degummed SF (5 g) was dissolved in 25 mL 9.3 mol·L^{-1} LiBr solution, and GMA of 296, 436, 571, and 700 mmol·L^{-1} was slowly dropped into the mixture and then stirred at 60 °C for 3 h. The prepared solution was dialyzed with a cellulose tubular membrane (molecular weight cut-off (MWCO): 14 000, St. Louis, USA) in distilled water for 3 d at room temperature, and then filtered as well as lyophilized to obtain SFMA sponges.

The degree of methacrylate (DM) in terms of the GMA concentration was detected by proton nuclear magnetic resonance spectroscopy (^{1}H-NMR) at a frequency of 600 MHz (Bruker, Germany) and a 5 mg sample was dissolved in 500 μL deuterium substituted water (D_2O). The DM was calculated based on the proton peak area of the lysine of SF ($P_{\text{lysine(SF)}}$, δ = 2.7–2.9) and that of SFMA ($P_{\text{lysine(SFMA)}}$, δ = 2.8–3.0), and the equation was as follows:

$$\text{DM}/\% = \left(1 - \frac{P_{\text{lysine(SFMA)}}}{P_{\text{lysine(SF)}}}\right) \times 100 \quad (1)$$

2.3 Preparation of hybrid 3D nanofibrous scaffolds

The fabrication of SFMA/P(LLA-CL)–PEGDA hybrid 3D nanofibrous scaffolds incorporates following critical processes as illustrated in Fig. 1:

1) Fabrication of SFMA/P(LLA-CL) (8:2) 2D nanofibrous membranes. The detailed fabricating process is presented in the section of electronic supplementary information (ESI).

2) Cutting SFMA/P(LLA-CL) (8:2) 2D nanofibrous membranes into small fragments.

3) Adding SFMA/P(LLA-CL) nanofibers fragments, PEGDA, photoinitiator LAP, and t-BuOH into a beaker and homogenizing with IKA T-18 at 10 000–12 000 r·min^{-1} for 60 min to fabricate dispersions (the mass ratios of SFMA/P(LLA-CL) nanofibers fragments to PEGDA were 10:0, 9:1, 8:2, 7:3, and 5:5). In the pre-experiment, it was found that the dissolved weight ratio

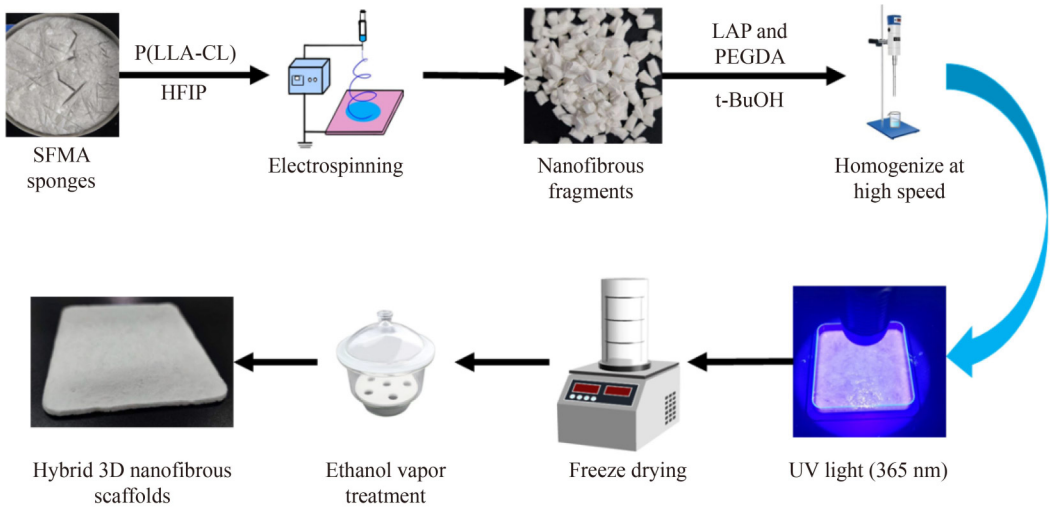

Fig. 1 Scheme of SFMA/P(LLA-CL)–PEGDA hybrid 3D nanofibrous scaffolds processing steps.

(DWR) in deionized water of SFMA/P(LLA-CL)–PEGDA (5:5) hybrid 3D nanofibrous scaffolds was more than 40%. So, the mass ratio 5:5 of SFMA/P(LLA-CL) to PEGDA was not used for the subsequent experimental research. The content of LAP was 5% of the total mass of SFMA/P(LLA-CL) nanofibrous fragments and PEGDA. The concentration of dispersions was about 2 wt.%.

4) Removal of the dispersions into the petri dish and irradiation for 10 min with the 365 nm ultraviolet (UV) light-emitting diode (LED) light.

5) Freeze-drying for 48 h to obtain SFMA/P(LLA-CL)–PEGDA hybrid 3D nanofibrous scaffolds, followed by post-treatment with 75% ethanol vapor for 2 h to further change the SFMA conformation from water-soluble random coil to water-insoluble β-sheet. The residual solvent on samples was detached in a vacuum drying oven.

2.4 Characterization

The cross-sectional and lengthwise sectional morphologies of SFMA/P(LLA-CL)–PEGDA hybrid 3D nanofibrous scaffolds were observed by scanning electron microscopy (SEM; S-4800, Hitachi, Japan) at an acceleration voltage of 10 kV. The chemical structure of the samples was characterized using Fourier transform infrared spectroscopy-attenuated total reflectance (FTIR-ATR; V70, Bruker, Germany). Thermogravimetric (TG) and differential thermogravimetric (DTG) analyses were performed using thermogravimetric analyzer (TA Q50, USA) at a heating rate of 10 °C·min^{-1} from room temperature to 800 °C. The microstructure of hybrid 3D nanofibrous scaffolds was investigated using a Desk-top X-ray microtomography (micro-computed tomography (micro-CT); SkyScan-1272, Bruker, Germany) and reconstructed into 3D models via NRecon software (Bruker), and then the inter-microstructures were analyzed by CTAn software (Bruker).

2.5 Property determination of hybrid 3D nanofibrous scaffolds

The swelling water rate (SWR) and the DWR of hybrid 3D nanofibrous scaffolds were measured as described in Ref. [32], and the details are presented in the ESI.

Mechanical properties of hybrid 3D nanofibrous scaffolds were examined in a wet state. All scaffolds were soaked in phosphate-buffered saline (PBS) for 30 min before testing. The mechanical properties of hybrid 3D nanofibrous scaffolds were investigated by a material mechanical property tester (H5K-S, Hounsfield, UK) as described in Refs. [27,33], and the details are presented in the ESI.

The HUVECs proliferation on different hybrid 3D nanofibrous scaffolds was evaluated. The cells were cultured in Dulbecco's modified eagle medium (DMEM) supplemented with 10% fetal bovine serum (FBS) and 1% (v/v) antibiotic penicillin–streptomycin in a humidified atmosphere with 5% CO_2 at 37 °C. The different hybrid 3D nanofibrous scaffolds with the diameter of 14 mm were fixed into 24-well plates with a quartz ring, then disinfected with 75% ethanol vapor for 24 h, and blow-dried in a super clean table. The cells were seeded at a density of 1.0×10^4 per well onto 3D nanofibrous scaffolds

and tissue culture plates (TCPs). The cells proliferated for 1, 3, and 5 d, and the cell viability at each time point was evaluated by the 3-[4,5-dime hyl-2-thiazolyl]-2,5-diphenyl-2-H-tetrazolium bromide (MTT) assay.

The hybrid 3D nanofibrous scaffolds co-cultured with HUVECs for 3 d were rinsed three times with PBS and fixed in 2.5% glutaraldehyde aqueous solution at 4 °C for 2 h. The fixed samples were rinsed again for three times with PBS, then dehydrated in graded concentrations of ethanol (30%, 50%, 70%, 80%, 90%, 95%, and 100%), and finally freeze-dried. The morphology of cells on hybrid 3D nanofibrous scaffolds was observed by SEM at a voltage of 10 kV.

2.6 Statistical analysis

All the data presented were analyzed by the 9.0 Origin software and expressed as mean ± standard deviation (SD) of the mean. The student's *t*-test and one-way analysis of variance (ANOVA) were used. The statistical significance was set at $p < 0.05$, $p < 0.01$, and $p < 0.001$, separately.

3 Results and discussion

3.1 Characterization of SFMA

SFMA was synthesized by replacing the primary amine of SF with GMA. To explore the appropriate concentration of GMA, SFMA was fabricated through the addition of different concentrations of GMA in the range from 296 to 700 mmol·L^{-1} into the SF LiBr solution and recorded as SFMA-296, SFMA-436, SFMA-571, and SFMA-700, separately. The FTIR-ATR and ^{1}H-NMR characterization results of the prepared SFMA samples are shown in Fig. 2. The characteristic absorption peaks of regeneration silk fibroin (RSF) at 1640 cm^{-1} (amide I), 1535 cm^{-1} (amide II), and 1237 cm^{-1} (amide III) were assigned to the SF with random coil or α-helical conformation [34]. After the modification with GMA, the characteristic absorption peaks at 1640 cm^{-1} (amide I), 1535 cm^{-1} (amide II), and 1237 cm^{-1} (amide III) showed no apparent shift. Meanwhile, two new characteristic absorption peaks appeared at 1690 and 1291 cm^{-1}. The former was attributed to the carbonyl (C=O) stretching vibration peak in GMA, while the latter was attributed to the stretching vibration peak of CHOH generated after the ring-opening reaction between the epoxide group on GMA and the amino group (−NH_2) on SF [9]. The results indicated that GMA was successfully grafted onto SF without causing a conformation change of SF. The DM and ring-opening of epoxy on GMA through nucleophilic addition reactions between −NH_2 on lysine were evaluated by ^{1}H-NMR (Figs. 2(b) and 2(c)). Two new signal peaks at δ = 6.0 and 5.6 were observed after the modification with GMA, which were assigned to the signals resulting from two hydrogen nuclei in −CH=CH_2. The methyl (−CH_3) signal appeared obviously at δ = 1.8. In addition, the lysine methylene signal at δ = 2.8 was weakened by increasing the proportion of GMA relative to RSF, indicating the

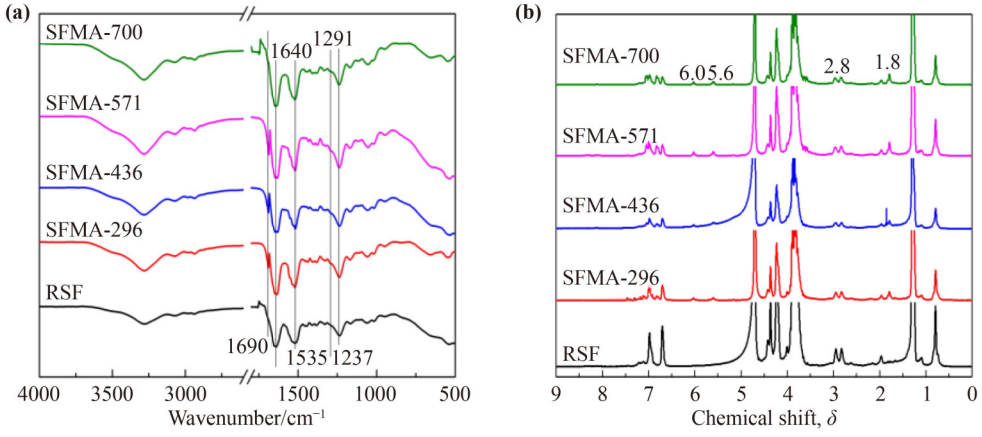

(c)

Samples	RSF	SFMA-296	SFMA-436	SFMA-571	SFMA-700
DM	0.00	50.59%	60.30%	40.75%	43.77%

Fig. 2 (**a**) FTIR-ATR spectra, (**b**) ^{1}H-NMR spectra, and (**c**) DMs of SFMA synthesized by replacing the primary amine of SF with different concentrations of GMA.

modification of lysine residues in SF. The DM value was the largest when the concentration of GMA reached 436 mmol·L^{-1}. Therefore, the GMA with 436 mmol·L^{-1} was applied to modify SF in subsequent experiments.

3.2 Effect of different crosslinking methods on hybrid 3D nanofibrous scaffolds

To obtain the "steel bar (nanofibers)–cement (PEGDA)" structure similar to ECM and improve mechanical properties, the SFMA/P(LLA-CL)–PEGDA hybrid 3D nanofibrous scaffolds were fabricated through the high-speed dispersion of sheared SFMA/P(LLA-CL) nanofibers, photoinitiator, and PEGDA into t-BuOH, followed by the template forming, then crosslinking with the 365 nm UV LED light, and finally freeze-drying. Three crosslinking polymerizations occurred, producing SFMA–SFMA, PEGDA–PEGDA, and SFMA–PEGDA, because there were two polymerization monomers in the reaction system [35] (Fig. S1). During the experiment, it was found that the SFMA/P(LLA-CL)–PEGDA hybrid 3D nanofibrous scaffolds only by photocrosslinking had a higher DWR value in water. Therefore, the SFMA/P(LLA-CL)–PEGDA hybrid 3D nanofibrous scaffolds were post-treated with 75% (v/v) ethanol vapor after freeze-drying. To enquire regarding the influence of different crosslinking methods on SFMA/P(LLA-CL)–PEGDA (8:2) hybrid 3D nanofibrous scaffolds, the DWR value in deionized water and the ART-FTIR result were measured under four different conditions: no light and no ethanol vapor treatment; light and no ethanol vapor treatment; no light and ethanol vapor treatment; light and ethanol vapor treatment. The results are shown in Fig. 3.

The DWR order of SFMA/P(LLA-CL)–PEGDA (8:2) hybrid 3D nanofibrous scaffolds for the four different crosslinking methods was: no light and no ethanol (59.08%) > light and no ethanol (52.47%) > no light and ethanol (26.24%) > light and ethanol (18.52%). Following conclusions could be drawn. Firstly, the PEGDA participated in the crosslinking polymerization reactions. The DWR would be at least more than 20% after light and vapor treatment if PEGDA did not participate in the reaction due to the fact that the mass ratio of SFMA/P(LLA-CL) nanofibers fragments to PEGDA was 8:2 and excessive LAP was also dissolved in deionized water, leading to an increase of DWR. Secondly, the water resistance for only photocrosslinking hybrid 3D nanofibrous scaffolds was significantly less than that for ethanol vapor treatment, which may be due to the fact that PEGDA only crosslinked with vinyl on SFMA and did not induce the conformational change of SF, while the ethanol vapor treatment induced the conformation of SF from random curl or α-helix to β-sheet structures [36]. To further seek the reason of the DWR change, the FTIR-ATR of SFMA/P(LLA-CL)–PEGDA hybrid 3D nanofibrous scaffolds with different crosslinking methods was investigated, and the results are shown in Fig. 3(b). Firstly, the hybrid 3D nanofibrous scaffolds 'without light and ethanol vapor treatment' showed characteristic absorption peaks at 1650 cm^{-1} (amide I), 1535 cm^{-1} (amide II), and 1240 cm^{-1} (amide III), attributable to the SF with water-soluble random coil or α-helical conformation [34]. The hybrid 3D nanofibrous scaffolds with 'only light and no ethanol vapor treatment' showed two peaks at 1650 and 1621 cm^{-1}, attributable to amide I, indicating that the conformations of partial SF from

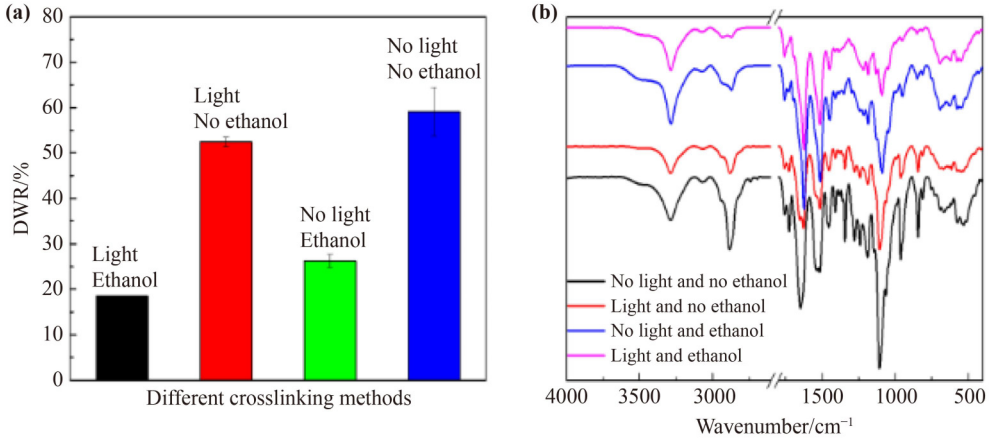

Fig. 3 (**a**) DWR and (**b**) FTIR-ATR results of SFMA/P(LLA-CL)–PEGDA hybrid 3D nanofibrous scaffolds with four different crosslinking methods.

random curls or α-helix to β-sheet structures. The hybrid 3D nanofibrous scaffolds with 'no light and ethanol vapor treatment' as well as 'light and ethanol vapor treatment' presented the characteristic absorption peak that could be assigned to amide I had shifted from 1650 to 1621 cm^{-1}, indicating that the 'ethanol vapor treatment' completely changed the conformations of SF from random curl or α-helix to water-insoluble β-sheet structures [34]. Some characteristic absorption peaks overlap each other in FTIR-ATR because hybrid 3D nanofibrous scaffolds contained SFMA, P(LLA-CL), PEGDA, and photoinitiator components. To probe the occurrence of the crosslinking polymerization reactions, taking the characteristic absorption peak at 1755 cm^{-1} (C=O) of P(LLA-CL) without participating in the photocrosslinking polymerization reaction as control, the ratio of characteristic absorption peak intensity at 810 cm^{-1} (attributed to the bending vibration of C−H ($CH=CH_2$) of PEGDA or SFMA) and that at 1755 cm^{-1} was used to diagnose the occurrence of a photocrosslinking polymerization reaction [37]. The ratio of the absorption peak intensity of 3D nanofibrous scaffolds 'with light' was lower than that of 'no light', indicating that the vinyl of PEGDA or SFMA participated in the photocrosslinking polymerization reaction [37]. FTIR-ATR and DWR results demonstrated that the combination of photocrosslinking and ethanol vapor post-treatment was a feasible method for the preparation of SFMA/P(LLA-CL)–PEGDA hybrid 3D nanofibrous scaffolds and the improvement of water resistance. The combination of photocrosslinking and ethanol vapor post-treatment was used for the fabrication of subsequent hybrid 3D nanofibrous scaffolds with different mass ratios of SFMA/P(LLA-CL) to PEGDA.

3.3 Thermal analyses of hybrid 3D nanofibrous scaffolds

TGA and DTG curves of the SFMA/P(LLA-CL)–PEGDA hybrid 3D nanofibrous scaffolds with different mass ratios of SFMA/P(LLA-CL) to PEGDA (from 10:0 to 7:3) are shown in Fig. 4. The SFMA/P(LLA-CL) 3D nanofibrous scaffolds presented two mass-loss stages, and the temperatures corresponding to the maximum mass-loss speed point ($T_{d,\,max}$) were 304.1 and 366.1 °C, attributed to the thermal decomposition of SF and P(LLA-CL) molecules, respectively [38]. The $T_{d,\,max}$ value attributed to the thermal decomposition of SF increased from 304.1 to 336.2 °C with the addition of PEGDA, while that attributed to the thermal decomposition of PEGDA increased from 396.9 to 414.8 °C with the increase of the PEGDA content [39]. The results not only demonstrated that the addition of PEGDA improved the thermal stability of SFMA and the thermal stability of PEGDA gradually with the increase of the PEGDA content in the hybrid 3D nanofibrous scaffolds, but also further confirmed the occurrence of the photocrosslinking reaction between PEGDA and SFMA as well as the self-photocrosslinking of PEGDA.

3.4 Morphologies and microstructures of hybrid 3D nanofibrous scaffolds

The cross-section and longitudinal-section morphologies of SFMA/P(LLA-CL)–PEGDA hybrid 3D nanofibrous scaffolds are shown in Fig. 5. All 3D nanofibrous scaffolds presented more remarkably porous 3D structures

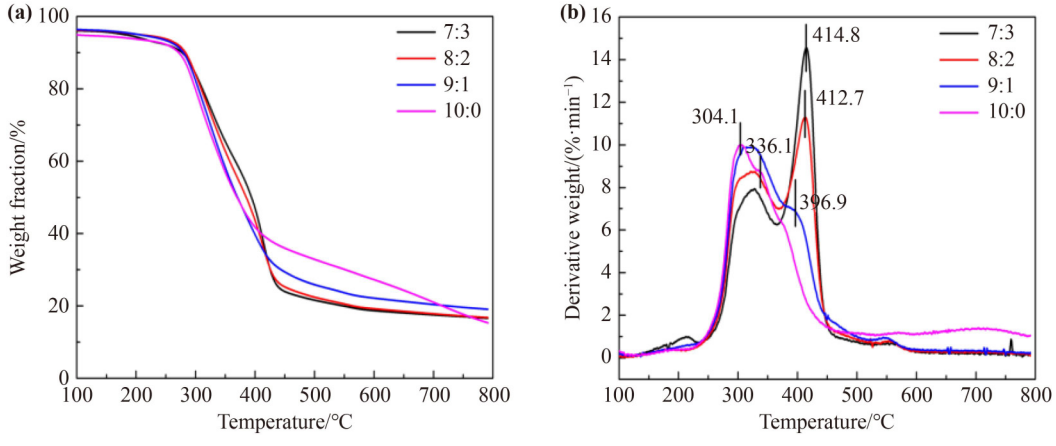

Fig. 4 (**a**) TGA and (**b**) DTG curves of SFMA/P(LLA-CL)–PEGDA hybrid 3D nanofibrous scaffolds with different mass ratios of SFMA/P(LLA-CL) to PEGDA.

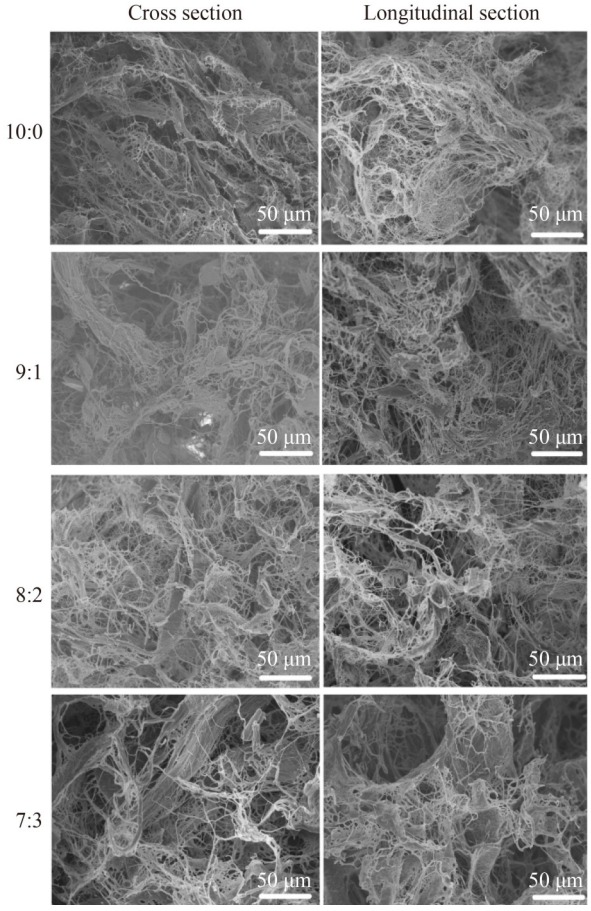

Fig. 5 SEM images of cross-section and longitudinal-section of SFMA/P(LLA-CL)–PEGDA hybrid 3D nanofibrous scaffolds with different mass ratios of SFMA/P(LLA-CL) to PEGDA.

with loosely packed nanofibers in comparison with 2D SFMA/P(LLA-CL) nanofibrous membrane (Fig. S2). Moreover, more PEGDA hydrogel-like matrices bonded nanofibers together to form a similar structure to the "steel bar (nanofiber)–cement (PEGDA)" one with the increase of the PEGDA content. This hierarchical structure was expected to realize the highly biomimetic natural ECM due to the fact that the natural ECM has a typical porous 3D structure of collagen, elastin, and fibronectin fibers with the diameter of 1–500 nm combined with hyaluronic acid and glucan gel [40–41]. In order to estimate finer details of the internal structure (including pore size, porosity, and pore connectivity density) of the 3D nanofibrous scaffolds, micro-CT was performed, and the results are shown in Fig. 6. The porosities of SFMA/P(LLA-CL)–PEGDA hybrid 3D nanofibrous scaffolds with different contents of PEGDA were slightly less than that of pure SFMA/P(LLA-CL) 3D nanofibrous scaffolds, but still more than 80%, and almost all pores within the scaffolds were open. It is seen that the pore connectivity densities of hybrid 3D nanofibrous scaffolds with different contents of PEGDA were less than that of pure SFMA/P(LLA-CL) 3D nanofibrous scaffolds. The reason may be that the addition of PEGDA into 3D nanofibrous scaffolds generated the PEGDA hydrogel-like matrix, which bonded short nanofibers together and blocked the connection between pores [42]. In contrast, their pore sizes were slightly larger than that of pure SFMA/P(LLA-CL) 3D nanofibrous scaffolds. In short, the addition of PEGDA had no obvious influence on the pore size and porosity of 3D nanofibrous scaffolds. This kind of porous 3D nanofibrous scaffolds not only promoted the diffusion of oxygen and related bioactive ingredients, but also stimulated the rapid adhesion and proliferation of corresponding cells in the materials [43]. Moreover, nanofibers could provide more adhesion sites for receptors on the cell membrane and cause changes in the focal adhesion (FA) of cells combining with nanofibers, as well as changes in the structure of the cytoskeleton inside cells, and can further influence the cell proliferation and differentiation behaviors [44]. Meanwhile, the PEGDA hydrogel-like matrix with high hydrophilicity and pliability provided a soft and moist microenvironment for the cell growth [45–46].

3.5 Swelling properties of hybrid 3D nanofibrous scaffolds

SWR and DWR values of the hybrid 3D nanofibrous scaffolds with different mass ratios of SFMA/P(LLA-CL) to PEGDA are revealed in Fig. 7. It is observed that the swelling properties of the hybrid 3D nanofibrous scaffolds were improved and the swelling equilibrium was arrived at more quickly with the change of the mass ratio of SFMA/P(LLA-CL) to PEGDA from 10:0 to 8:2. However, the swelling property decreased when the mass ratio further changed to 7:3. The lowered SWR of the SFMA/P(LLA-CL)–PEGDA (7:3) hybrid 3D nanofibrous scaffold may be due to that the increase of the crosslinking degree with the enhancement of the PEGDA content restrict the extension of molecular chains, which has an effect on the water absorption. Notably, this hybrid 3D nanofibrous scaffold of PEGDA hydrogel-like matrix combined with nanofibers enhanced the biofluids' absorbance to achieve a hydrophilic and soft microenvironment for cell ingrowth, and further provided a potential mechanical support to prevent squeezing from

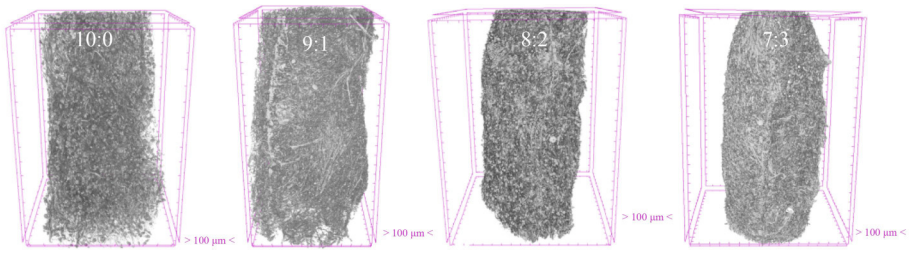

Property	10:0	9:1	8:2	7:3
Pore size/μm	17.528±6.821	23.492±8.917	30.843±13.879	19.316±7.349
Porosity/%	84.620±3.395	80.758±0.642	81.253±2.518	80.586±3.462
Open pore porosity/%	84.619±3.396	80.752±0.646	81.375±2.698	80.585±3.462
Closed pore porosity/%	0.006±0.001	0.030±0.023	0.014±0.016	0.002±0.001
Pore connectivity density/ (10^4 mm^{-3})	8.262±0.341	4.898±0.872	4.730±0.960	5.548±1.020

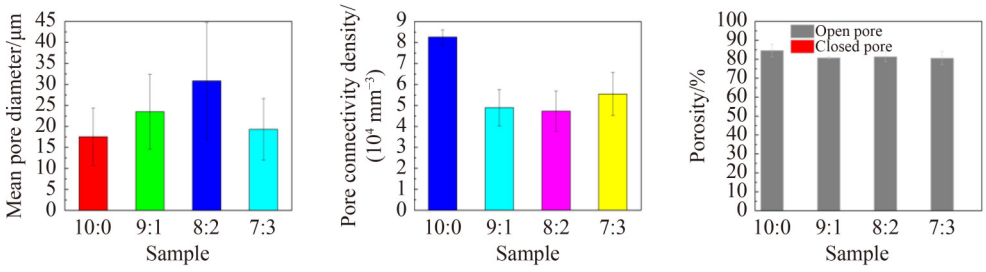

Fig. 6 Internal microstructure (including pore size, porosity, and pore connectivity density) of SFMA/P(LLA-CL)–PEGDA hybrid 3D nanofibrous scaffolds by micro-CT with different mass ratios of SFMA/P(LLA-CL) to PEGDA.

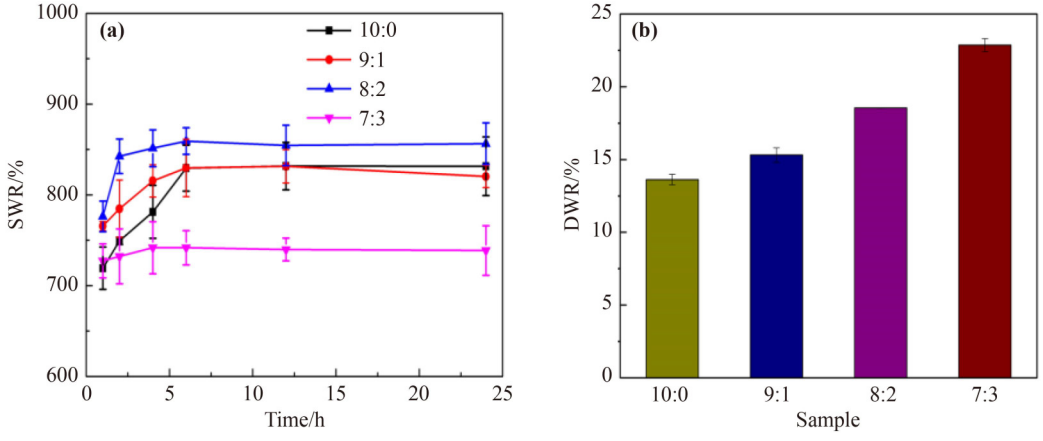

Fig. 7 (**a**) SWRs and (**b**) DWRs of SFMA/P(LLA-CL)–PEGDA hybrid 3D nanofibrous scaffolds with different mass ratios of SFMA/P(LLA-CL) to PEGDA.

surrounding tissues.

3.6 Mechanical properties of hybrid 3D nanofibrous scaffolds

Compressive properties under the compressive load with the cylindrical axis up to 80% deformation and tensile properties of the hybrid 3D nanofibrous scaffolds in wet state are shown in Fig. 8. The general shapes of compressive stress–strain curves for different hybrid 3D nanofibrous scaffolds in wet state were similar, and the compressive strength and the Young's modulus for hybrid 3D nanofibrous scaffolds gradually increased with the rise of the PEGDA content. Meanwhile, the typical tensile stress–strain curves for different hybrid 3D nanofibrous scaffolds in wet state presented a high level of flexibility.

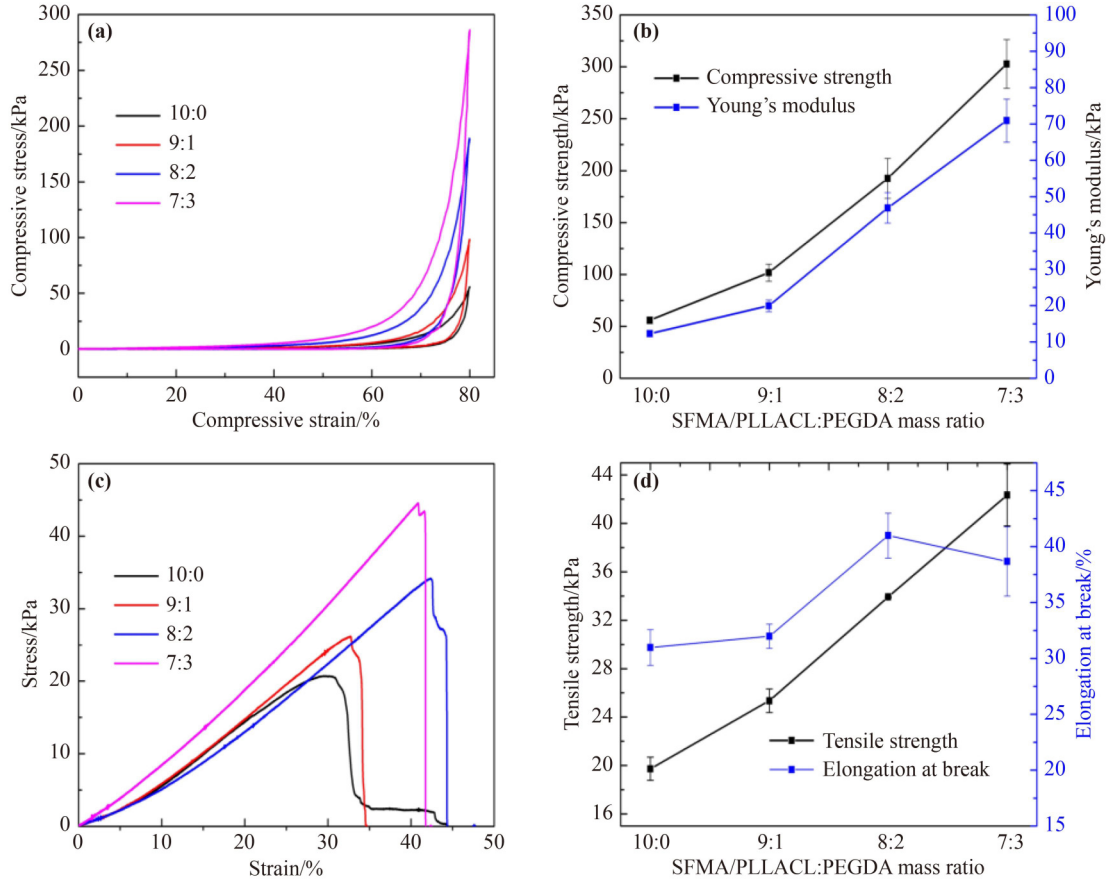

Fig. 8 (**a**)(**b**) Compressive properties and (**c**)(**d**) tensile properties of SFMA/P(LLA-CL)–PEGDA hybrid 3D nanofibrous scaffolds with different mass ratios of SFMA/P(LLA-CL) to PEGDA in wet state.

The average tensile strength obviously enhanced with the change of the mass ratio of SFMA/P(LLA-CL) to PEGDA in the range from 10:0 to 7:3, while the average elongation at break was firstly raised to 40.99% ± 2.01% and then slightly dropped to 38.68% ± 3.09% with changing the mass ratio of SFMA/P(LLA-CL) to PEGDA from 10:0 to 8:2 and then to 7:3. The results indicated that the addition of PEGDA could effectively strengthen the mechanical properties of hybrid 3D nanofibrous scaffolds, which could be credited to the crosslinking and bonding function of PEGDA hydrogel-like matrices on short SFMA/P(LLA-CL) nanofibers in the SFMA/P(LLA-CL)–PEGDA hybrid 3D nanofibrous scaffolds. The improvement of mechanical properties was of great significance for applying such 3D nanofibrous scaffolds in tissue engineering. These hybrid 3D nanofibrous scaffolds not only maintained their porous 3D nanofibrous morphologies by ensuring sufficient mechanical properties in the body, but also achieved the natural ECM-like structural support for cell in-growth and matrix production [42].

3.7 *In vitro* biocompatibility of hybrid 3D nanofibrous scaffolds

To investigate the biocompatibility of SFMA/P(LLA-CL)–PEGDA hybrid 3D nanofibrous scaffolds, the proliferation of HUVECs on different 3D nanofibrous scaffolds was examined by the MTT method, and the results are shown in Fig. 9. The cell proliferation on SFMA/P(LLA-CL)–PEGDA (9:1) and (7:3) hybrid 3D nanofibrous scaffolds presented significant increase ($p < 0.01$ and $p < 0.001$) compared to those on the pure SFMA/P(LLA-CL) 3D nanofibrous scaffold and the TCP at day 1, respectively. On day 3, the cell proliferation on all SFMA/P(LLA-CL)–PEGDA hybrid 3D nanofibrous scaffolds showed significant difference ($p < 0.01$ and $p < 0.05$) compared to that on the TCP. In addition, the cell proliferation on SFMA/P(LLA-CL)–PEGDA (9:1 and 8:2) 3D nanofibrous scaffolds had significant difference ($p < 0.01$ and $p < 0.05$) compared to that on the pure SFMA/P(LLA-CL) 3D nanofibrous scaffold. On day 5, the cell proliferation on all SFMA/P(LLA-CL)–PEGDA

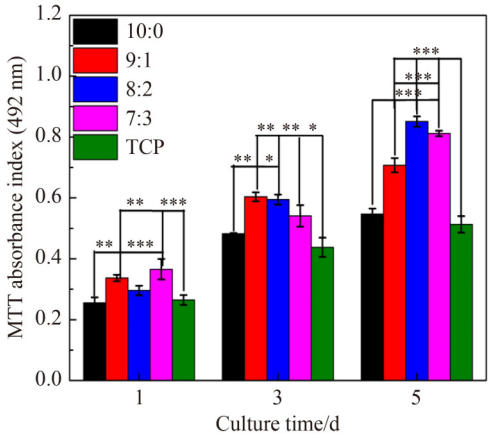

Fig. 9 Proliferation of HUVECs on SFMA/P(LLA-CL)–PEGDA hybrid 3D nanofibrous scaffolds with different mass ratios of SFMA/P(LLA-CL) to PEGDA (* $p < 0.05$; ** $p < 0.01$; *** $p < 0.001$).

hybrid 3D nanofibrous scaffolds had significant difference ($p < 0.001$) compared with those on the TCP and the pure SFMA/P(LLA-CL) 3D nanofibrous scaffold. The results demonstrated that all SFMA/P(LLA-CL)–PEGDA hybrid 3D nanofibrous scaffolds were more favorable for the HUVECs proliferation than the pure SFMA/P(LLA-CL) 3D nanofibrous scaffold. The addition of PEGDA endowed not only a porous 3D nanofibrous structure but also characteristics of hydrogel such as elasticity and less interfacial stress with water and other biofluids, leading to high similarity to the structure of ECM with more hydrophilicity and higher stiffness [47]. It is recognized that an ECM-like microenvironment greatly enhance the cell proliferation. To further investigate the interaction between HUVECs and hybrid 3D nanofibrous scaffolds, the morphologies of 3D nanofibrous scaffolds seeded with HUVECs for 3 d were examined by SEM, and the results are shown in Fig. 10. HUVECs on all 3D nanofibrous scaffolds displayed well spread morphologies and well integrated with peripheral nanofibers. Numerous pseudopodia, extending from the edge of the cell body, produced fusion of cells with the surrounding nanofibers to facilitate intracellular communication and promote cell adhesion as well as migration by providing anchoring points [48]. In addition, some cells migrated to nanofibers inside SFMA/P(LLA-CL)–PEGDA hybrid 3D nanofibrous scaffolds (white arrows, Fig. 10), especially when the mass ratio of SFMA/P(LLA-CL) to PEGDA was 8:2, resembling the cell adhesion and growth on fibers inside natural ECM [49]. This phenomenon manifested in mimicry by SFMA/P(LLA-CL)–PEGDA hybrid 3D nanofibrous scaffolds of the ECM structure,

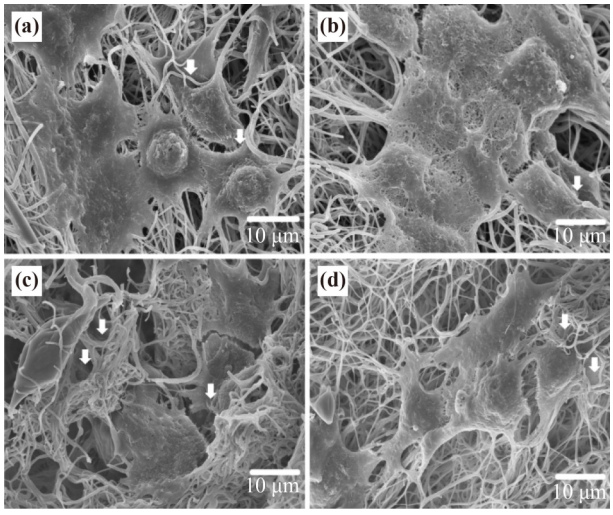

Fig. 10 SEM images of HUVECs grown on SFMA/P(LLA-CL)–PEGDA hybrid 3D nanofibrous scaffolds with different mass ratios of SFMA/P(LLA-CL) to PEGDA for 3 d: (**a**) 10:0; (**b**) 9:1; (**c**) 8:2; (**d**) 7:3.

providing nano-scale adhesion sites for cells to sense external forces [50].

4 Conclusions

A novel porous hybrid 3D nanofibrous scaffold similar to the "steel bar (nanofiber)–cement (PEGDA)" structure was successfully fabricated and exhibited better hydrophilic and mechanical properties than those of the pure SFMA/P(LLA-CL) 3D nanofibrous scaffold. Moreover, *in vitro* results demonstrated that the hybrid 3D nanofibrous scaffolds possessed more outstanding cytocompatibility. Ongoing studies will be further focused on exploring the interaction between scaffolds and cells from the perspective of molecular biology. The hybrid 3D nanofibrous scaffold with PEGDA hydrogel-like matrices is expected to fabricate different shapes and sizes using different molds for soft tissue repair and regeneration.

Disclosure of potential conflicts of interests The authors declare no conflict of interest.

Acknowledgements This work was sponsored by the Jiaxing Public Welfare Research Project (Grant Nos. 2021AY10062 and 2021AY10063), the Zhejiang Provincial Natural Science Foundation of China (Grant Nos. LY20C100003 and LY22C100001), and the National Undergraduate Training Program for Innovation and Entrepreneurship (Grant No. 202010354009).

Electronic supplementary information Supplementary materials can be found in the online version at https://doi.org/10.1007/s11706-023-0647-7, which include Figs. S1–S2.

References

[1] Zhong H, Huang J, Wu J, et al. Electrospinning nanofibers to 1D, 2D, and 3D scaffolds and their biomedical applications. Nano Research, 2022, 15(2): 787–804

[2] Yao Q, Fuglsby K E, Zheng X, et al. Nanoclay-functionalized 3D nanofibrous scaffolds promote bone regeneration. Journal of Materials Chemistry B: Materials for Biology and Medicine, 2020, 8(17): 3842–3851

[3] Xie X R, Chen Y J, Wang X Y, et al. Electrospinning nanofiber scaffolds for soft and hard tissue regeneration. Journal of Materials Science and Technology, 2020, 59: 243–261

[4] Laschke M W, Menger M D. Prevascularization in tissue engineering: current concepts and future directions. Biotechnology Advances, 2016, 34(2): 112–121

[5] Pan D, Mackinnon S E, Wood M D. Advances in the repair of segmental nerve injuries and trends in reconstruction. Muscle & Nerve, 2020, 61(6): 726–739

[6] Rodriguez M J, Brown J, Giordano J, et al. Silk based bioinks for soft tissue reconstruction using 3-dimensional (3D) printing with *in vitro* and *in vivo* assessments. Biomaterials, 2017, 117: 105–115

[7] Chouhan D, Dey N, Bhardwaj N, et al. Emerging and innovative approaches for wound healing and skin regeneration: current status and advances. Biomaterials, 2019, 216: 119267

[8] Kim S H, Yeon Y K, Lee J M, et al. Precisely printable and biocompatible silk fibroin bioink for digital light processing 3D printing. Nature Communications, 2018, 9(1): 1620

[9] Fan L, Li J L, Cai Z, et al. Creating biomimetic anisotropic architectures with co-aligned nanofibers and macrochannels by manipulating ice crystallization. ACS Nano, 2018, 12(6): 5780–5790

[10] Lin M, Xie W, Cheng X, et al. Fabrication of silk fibroin film enhanced by acid hydrolyzed silk fibroin nanowhiskers to improve bacterial inhibition and biocompatibility efficacy. Journal of Biomaterials Science: Polymer Edition, 2022, 33(10): 1308–1323

[11] Lin N, Zuo B. Silk sericin/fibroin electrospinning dressings: a method for preparing a dressing material with high moisture vapor transmission rate. Journal of Biomaterials Science: Polymer Edition, 2021, 32(15): 1983–1997

[12] Wang C, Jia Y, Yang W, et al. Silk fibroin enhances peripheral nerve regeneration by improving vascularization within nerve conduits. Journal of Biomedical Materials Research Part A, 2018, 106(7): 2070–2077

[13] Zhang K, Qian Y, Wang H, et al. Genipin-crosslinked silk fibroin/hydroxybutyl chitosan nanofibrous scaffolds for tissue-engineering application. Journal of Biomedical Materials Research Part A, 2010, 95A(3): 870–881

[14] Chen Y, Dong X, Shafiq M, et al. Recent advancements on three-dimensional electrospun nanofiber scaffolds for tissue engineering. Advanced Fiber Materials, 2022, 4(5): 959–986

[15] Qasim M, Chae D S, Lee N Y. Advancements and frontiers in nano-based 3D and 4D scaffolds for bone and cartilage tissue engineering. International Journal of Nanomedicine, 2019, 14: 4333–4351

[16] Chen W M, Xu Y, Liu Y Q, et al. Three-dimensional printed electrospun fiber-based scaffold for cartilage regeneration. Materials & Design, 2019, 179: 107886

[17] Bongiovanni Abel S, Montini Ballarin F, Abraham G A. Combination of electrospinning with other techniques for the fabrication of 3D polymeric and composite nanofibrous scaffolds with improved cellular interactions. Nanotechnology, 2020, 31(17): 172002

[18] Koyyada A, Orsu P. Recent advancements and associated challenges of scaffold fabrication techniques in tissue engineering applications. Regenerative Engineering and Translational Medicine, 2021, 7(2): 147–159

[19] Juran C M, Dolwick M F, McFetridge P S. Engineered microporosity: enhancing the early regenerative potential of decellularized temporomandibular joint discs. Tissue Engineering Part A, 2015, 21(3–4): 829–839

[20] Zhang J, Zhou A, Deng A, et al. Pore architecture and cell viability on freeze dried 3D recombinant human collagen-peptide (RHC)-chitosan scaffolds. Materials Science and Engineering C, 2015, 49: 174–182

[21] Somo S I, Akar B, Bayrak E S, et al. Pore interconnectivity influences growth factor-mediated vascularization in sphere-templated hydrogels. Tissue Engineering Part C: Methods, 2015, 21(8): 773–785

[22] Jin G, He R, Sha B, et al. Electrospun three-dimensional aligned nanofibrous scaffolds for tissue engineering. Materials Science and Engineering C, 2018, 92: 995–1005

[23] Keirouz A, Chung M, Kwon J, et al. 2D and 3D electrospinning technologies for the fabrication of nanofibrous scaffolds for skin tissue engineering: a review. Wiley Interdisciplinary Reviews - Nanomedicine and Nanobiotechnology, 2020, 12(4): e01626

[24] Wang J, Cheng Y, Wang H, et al. Biomimetic and hierarchical nerve conduits from multifunctional nanofibers for guided peripheral nerve regeneration. Acta Biomaterialia, 2020, 117: 180–191

[25] Xu T, Miszuk J M, Zhao Y, et al. Electrospun polycaprolactone 3D nanofibrous scaffold with interconnected and hierarchically structured pores for bone tissue engineering. Advanced Healthcare Materials, 2015, 4(15): 2238–2246

[26] Sun B, Zhou Z, Wu T, et al. Development of nanofiber sponges-containing nerve guidance conduit for peripheral nerve regeneration *in vivo*. ACS Applied Materials & Interfaces, 2017, 9(32): 26684–26696

[27] Shen J, Wang J, Liu X, et al. *In situ* prevascularization strategy with three-dimensional porous conduits for neural tissue engineering. ACS Applied Materials & Interfaces, 2021, 13(43): 50785–50801

[28] Doustdar F, Olad A, Ghorbani M. Effect of glutaraldehyde and calcium chloride as different crosslinking agents on the characteristics of chitosan/cellulose nanocrystals scaffold. International Journal of Biological Macromolecules, 2022, 208: 912–924

[29] Yu X, Zhang T, Li Y. 3D printing and bioprinting nerve conduits for neural tissue engineering. Polymers, 2020, 12(8): 1637

[30] Liu J, Zhang B, Li L, et al. Additive-lathe 3D bioprinting of bilayered nerve conduits incorporated with supportive cells. Bioactive Materials, 2021, 6(1): 219–229

[31] Zhu W, Tringale K R, Woller S A, et al. Rapid continuous 3D printing of customizable peripheral nerve guidance conduits. Materials Today, 2018, 21(9): 951–959

[32] Zhou X, Yin A, Sheng J, et al. *In situ* deposition of nano Cu_2O on electrospun chitosan nanofibrous scaffolds and their antimicrobial properties. International Journal of Biological Macromolecules, 2021, 191: 600–607

[33] Chen Y, Xu W, Shafiq M, et al. Chondroitin sulfate cross-linked three-dimensional tailored electrospun scaffolds for cartilage regeneration. Biomaterials Advance, 2022, 134: 112643

[34] Chen X, Shao Z, Marinkovic N S, et al. Conformation transition kinetics of regenerated *Bombyx mori* silk fibroin membrane monitored by time-resolved FTIR spectroscopy. Biophysical Chemistry, 2001, 89(1): 25–34

[35] Wang Y H, Zhang B, Ma M, et al. Synthesis of GelMA/PEGDA hydrogel by UV photopolymerization. Imaging Science and Photochemistry, 2017, 35(4): 574–580 (in Chinese)

[36] Bae S B, Kim M H, Park W H. Electrospinning and dual crosslinking of water-soluble silk fibroin modified with glycidyl methacrylate. Polymer Degradation & Stability, 2020, 179: 109304

[37] Zeng R X. Modern Testing and Analysis Technology of Polymers. Guangzhou, China: South China University of Technology Press, 2007

[38] Zhang K H, Yin A L, Huang C, et al. Degradation of electrospun SF/P(LLA-CL) blended nanofibrous scaffolds *in vitro*. Polymer Degradation & Stability, 2011, 96(12): 2266–2275

[39] Ma G, Zhang X, Han J, et al. Photo-polymeriable chitosan derivative prepared by Michael reaction of chitosan and polyethylene glycol diacrylate (PEGDA). International Journal of Biological Macromolecules, 2009, 45(5): 499–503

[40] Feng J, Wang F, Han X, et al. A "green pathway" different from simple diffusion in soft matter: fast molecular transport within micro/nanoscale multiphase porous systems. Nano Research, 2014, 7(3): 434–442

[41] Li K, Zhu Y, Zhang Q, et al. A self-healing hierarchical fiber hydrogel that mimics ECM structure. Materials, 2020, 13(22): 5277

[42] Mirtaghavi A, Baldwin A, Tanideh N, et al. Crosslinked porous three-dimensional cellulose nanofibers–gelatine biocomposite scaffolds for tissue regeneration. International Journal of Biological Macromolecules, 2020, 164: 1949–1959

[43] Somo S I, Akar B, Bayrak E S, et al. Pore interconnectivity influences growth factor-mediated vascularization in sphere-templated hydrogels. Tissue Engineering Part C: Methods, 2015, 21(8): 773–785

[44] Higgins A M, Banik B L, Brown J L. Geometry sensing through POR1 regulates Rac1 activity controlling early osteoblast differentiation in response to nanofiber diameter. Integrative Biology, 2015, 7(2): 229–236

[45] Sharma S, Tiwari S. A review on biomacromolecular hydrogel classification and its applications. International Journal of Biological Macromolecules, 2020, 162: 737–747

[46] Zhao X D, Pei D D, Yang Y X, et al. Green tea derivative driven smart hydrogels with desired functions for chronic diabetic wound treatment. Advanced Functional Materials, 2021, 31(18): 2009442

[47] Ansar R, Saqib S, Mukhtar A, et al. Challenges and recent trends with the development of hydrogel fiber for biomedical applications. Chemosphere, 2022, 287(Pt 1): 131956

[48] McClay D R. The role of thin filopodia in motility and morphogenesis. Experimental Cell Research, 1999, 253(2): 296–301

[49] Prince E, Kumacheva E. Design and applications of man-made biomimetic fibrillar hydrogels. Nature Reviews Materials, 2019, 4(2): 99–115

[50] Spang M T, Christman K L. Extracellular matrix hydrogel therapies: *in vivo* applications and development. Acta Biomaterialia, 2018, 68: 1–14